FULLY FEM-BASED SIMULATION APPROACH FOR ADVANCED HELICOPTER INTERIOR NOISE DESIGN USING NOISE SOURCES EXTRACTED FROM FLIGHT TEST DATA

Nicolai Stadlmair, Daniel Redmann

Kopter Germany GmbH, Altlaufstr. 34, 85635 Höhenkirchen-Siegertsbrunn, Germany
nicolai.stadlmair@koptergroup.de

ABSTRACT

Apart from exterior noise emissions which are subject of the type certification of a helicopter, also the noise perception inside the cabin poses major design challenges in rotorcraft development. In particular, rotating components such as rotors, drive shafts, engine components and gears are commonly known sources of sound. Of particular relevance are those sources whose frequency range interferes with that of human voice, for which the Speech Interference Level (SIL) is a widely used metric. In the recent past, availability of computational resources as well as development of efficient and robust numerical solution methods have experienced a steep gradient. This paves the way for the use of Fine Element Methods (FEM) to simulate acoustic wave propagation for successively higher frequencies in ever larger volumes such as helicopter cabins. With the aim of designing effective measures to optimize the SIL4 noise level of a helicopter cabin we present the applicability of a full FEM-based acoustics simulation approach. The presented model is capable to cover the full frequency range bounded by the SIL4 range. To describe location and strength of the acoustic sources, we exploit measurement data recorded during regular flight test campaigns allowing to compute equivalent accelerations for the major sources of sound. Using the AW09 prototype helicopter as a practical example, the acoustic performance in terms of SIL4 reduction is investigated for two treated configurations: One with a carpet and a second with carpet and a ceiling panel. The materials are acoustically described by frequency-dependent absorption coefficients from literature. As a result, the reduction potential of the carpet is quantified to range between $\approx$ 1.2 and 1.8 SIL4dB and up to approx. 11.5 SIL4dB for the case with carpet and ceiling panel. The great potential of model lies in its implementation in a multiphysics simulation environment. This allows for example to include more complex interaction effects such as acoustic-structure coupling as well as consideration of structures like acoustic metamaterials.

NOMENCLATURE

Symbols

a	surface normal acceleration
α	surface absorption coefficient
c	speed of sound
f	frequency
f_c	one-third octave band center frequency
k_{ij}	cross-correlation function
l	length
L_P	Sound pressure level
$\mathbf{n}$	surface normal vector
ω	angular frequency
p	pressure
ρ	density
R	reflection coefficient
t	time
v_n	surface normal velocity component
Z_i	specific acoustic impedance

Indices

$[\dots]_A$	accelerometer
$[\dots]_0$	environment fluid
$[\dots]_c$	center
$[\dots]_M$	microphone
$[\dots]_{\text{max}}$	maximum
$[\dots]_{\text{min}}$	minimum
$[\dots]_{\text{oct}}$	octave band

Presented at 48th European Rotorcraft Forum, Winterthur, Switzerland, 6-8th September, 2022

1 INTRODUCTION

While exterior noise emissions are part of the type certification of a helicopter, interior low noise design is mainly driven by passenger comfort. The most important sources of sound perceived inside the cabin are usually rotating components such as rotors, drive shafts, engine components and gears. Many of these sources induce vibrations which are transferred by the structure of the helicopter cabin to the interior leading to a significant exposure of passengers and crew to high levels of noise [1, 2]. As a major design goal, crew and passengers must be able to communicate and therefore special attention is paid to such noise interfering with human voice due to its characteristic frequencies. In this context, a frequently used noise metric is the Speech Interference Value (SIL). It is thus one of the primary targets of the helicopters' acoustic design to keep the noise levels within this range in the passenger compartment to a minimum in such a way that safety and comfort of the crew is ensured at all times. To achieve this goal, appropriate design and measures should be as lightweight as possible while keeping costs to a minimum. It is well known that in most conventional helicopters, the gearbox is among the main sources of interior noise. Therefore, many studies are available on the acoustic optimization of the transmission system, such as [3, 4, 5].

For an effective acoustically sophisticated design, it is essential to reduce iterations of the design-build-test cycle. Therefore, the use of computer simulations for design optimization, especially in the early development phases of the product is key. In this context, it is well known that a spatially highly resolved solution of oscillation problems, as they also occur in helicopter interior acoustics can be obtained by using Finite Element Modelling (FEM). In the past, however, this was usually only applicable to low-frequency problems, since there the frequencies are sufficiently small to satisfy a resolution of 6-8 elements per wavelength. This resolution is usually required when considering accuracy, system complexity and computational power [6]. Oscillation problems at medium frequencies (in the order of hundreds of Hertz) are often subject to use of Boundary Element Methods (BEM), whereby complexly structured surfaces, such as those found in helicopters, often create particular difficulties to the numerical solution algorithms. Last but not least, resolving frequencies of several thousand Hertz with a high spatial resolution poses a major challenge to numerical simulation. The sound field of the relevant frequencies in a helicopter cabin usually comprises all three frequency ranges mentioned. Based on the assumption that mid- and high-frequency acoustic airborne noise sources are uncorrelated and can be described as statistically independent in models, Statistical Energy Analysis (SEA) is often used to solve acoustic problems in aviation [7, 8]. Further developments go in the direction of hybrid SEA methods by considering virtual measurement data, where low frequencies are computed with a modal FEM approach while higher frequencies are considered via SEA [9, 10]. One drawback of this method is that it can only be robustly used on existing designs or structures, since coupling and damping factors as well as the main transfer paths need to be known. This usually requires dedicated measurements, e.g. transfer path analysis [11, 12], which are very time consuming and costly as they require special test vehicles, environment and equipment. Otherwise, these values must be determined either by use of supplementary methodologies or by making engineering assumptions. Among other things, this hampers the use in an early product phase due to higher degrees of uncertainty. Another way to simulate the full frequency spectrum is to use different methods (FEM, BEM and Ray tracing) depending on the frequency range. However, this increases the modeling effort since different models have to be used depending on the method and boundary conditions have to be defined differently. In the recent past, the increasing availability of computational resources as well as a steep gradient in the development of efficient and robust numerical solution methods now allow the use of a fully FEM-based modelling approach for acoustic wave propagation in large volumes [13].

Inspired by the rising trend towards the intensified use of FEM for interior acoustics simulation in the automotive sector (see e.g. Kun et al. [14] for an extensive overview), we demonstrate in this study the applicability of FEM simulations for a helicopter cabin capable to investigate complex geometries and materials. To determine location and strength of the most relevant acoustic sources, we exploit measurement data recorded during regular test flights. More specifically, a modal reconstruction of the sound pressure field inside the helicopter cabin is used based on a small number of measurements positions. Similar methods are e.g. described in [15] and [16]. For this purpose, the latest generation of solver algorithms for the acoustic governing equations implemented in the COMSOL Multiphysics® simulation software[17] are used. By using the AW09's cabin as an illustrative example, we will present a modeling framework that is applicable for the full frequency range of the SIL4 index. From an industrial viewpoint, the main purpose of the model is to equip the rotorcraft with specific and appropriate measures to reduce the im-

pact of the tonal components. In particular, it should allow to make statements on the choice of the right material and its optimal placement in order to realize a maximum sound reduction at given locations with a minimum of weight. The aim of the paper is to demonstrate functionality, outline plausibility of the results and highlight the potential with the new simulation environment.

2 THEORY

In the following, the governing acoustic equation implemented in the FEM-based simulation approach will be briefly derived. Firstly, the used formulation of the Helmholtz equation for acoustic wave propagation in the frequency space formulation will be described. Subsequently, the realization of the boundary conditions via specific acoustic impedance is presented. The used solving algorithms are outlined afterwards. Finally, a brief overview on the used noise metrics is given.

2.1 Helmholtz-Equations in frequency space

To solve acoustic problems with Finite Element Methods (FEM), the solution of the Helmholtz Equations formulated in frequency space is a common approach. Starting from the time domain, the equations that describe the propagation of sound in fluids can be derived from the governing equations of fluid flow. That is, conservation of mass, momentum, and energy. Additional equations of the state of the model itself and an equation of state to describe the relation between thermodynamic variables are used. The flow is assumed as lossless and adiabatic, viscous effects are neglected and a linearized isentropic equation of state is used. Under these assumptions, the acoustic field can be described by the pressure only which is governed by the wave equation, formulated in the time domain [18]:

$$\frac{1}{\rho_0 c^2}\frac{\partial^2 p}{\partial t^2} + \nabla \cdot \left(-\frac{1}{\rho_0}\nabla p\right) = 0. \tag{1}$$

Acoustic problems are often related to tonal components, which can be described by simple harmonic waves such as sinusoidal waves. Those, in turn, can be decomposed into harmonic components via their Fourier series. Thus, the wave equation can be solved in the frequency domain for each frequency of interest. For this purpose, the harmonic solutions can be decomposed into a spatial and a temporal part using the complex formulation of the pressure variable:

$$p(\vec{x},t) = p(\vec{x}) \cdot \exp(i\omega t), \tag{2}$$

where the real part of the above mentioned equation represents the instantaneous physical value of the pressure. Using this assumption for the pressure field, the time-dependent wave equation (Eq. 1) can be expressed in the frequency space by the well-known Helmholtz equation:

$$\nabla \cdot \left(-\frac{1}{\rho_0}\nabla p\right) - \frac{\omega^2}{\rho_0 c^2} p = 0. \tag{3}$$

2.2 Specific acoustic impedance

To describe the acoustic reflection and absorption behavior at the model boundaries, impedance boundary conditions are used. Thus, for ar a given surface, the acoustic pressure p and the acoustic velocity u can be related to each other. This relationship is provided by knowledge about the conditions on the boundary, for example, a specific material or an acoustically forced boundary. Therefore, an impedance boundary condition can be used to impose the properties of the boundary without modeling it explicitly. Impedance boundary conditions thus generalize the sound-hard and sound-soft boundary conditions to address a large number of cases between these two extremes.
Mathematically, a specific acoustic impedance Z_i is defined on some cross section as the ratio between the acoustic pressure p and the acoustic velocity perpendicular to the area $v_\perp$, the normal velocity [18]:

$$Z_i = \frac{p}{v_\perp}. \tag{4}$$

For pressure acoustics in the frequency domain, this boundary condition is imposed according to:

$$-\mathbf{n} \cdot \left(\frac{1}{\rho_0}(\nabla p - \mathbf{q}_d)\right) = \frac{i\omega p}{Z_i}. \tag{5}$$

The specific acoustic impedance can be expressed using the acoustic reflection coefficient of a surface R:

$$Z_i = \rho_0 c_0 \frac{1+R}{1-R}. \tag{6}$$

In practice, acoustic properties of absorbing surfaces are often only described by their acoustic absorption

coefficient α, which correlates to the reflection coefficient according to:

$$|R| = \sqrt{1-\alpha}. \tag{7}$$

When using the absorption coefficient by inserting Eq. 7 into Eq. 6 to describe the impedance, Z_i becomes real valued since no phase information is provided. While this approximation is considered acceptable at higher frequencies, results in the low frequency range should be considered with greater caution. In the latter case, the phase shift caused by a boundary condition can have a significant influence on the acoustic field.

2.3 Numerical solvers

In order to solve the discretized form of Equation 3 numerically, various approaches are known (see e.g. [13]). One popular linear solving algorithm for this kind of problems is the Multifrontal Massively Parallel Sparse Direct Solver (MUMPS). This method allows efficient and robust solution of the equation systems. The advantage here is the included out-of core solver, which stores the lower-upper (LU) factors of the system matrix according to

$$A = LU \tag{8}$$

on the hard disk to minimize the internal memory requirements. The MUMPS solver is an established direct linear system solver in the field of FEM and is known for is robustness. While the LU factorization is known as the computationally most expensive step of this process, the memory requirements increase quickly with increasing number of Degrees of Freedom (DOF). Hence, the use for acoustic problems for higher frequencies is limited to the order of 2-3 kHz, considering main memories in the order of several hundreds of gigabytes. More information on the performance of the MUMPS solver can e.g. be found in [20]. For higher frequencies, iterative solvers using Geometric Multigrid (GMG) or Algebraic Multigrid (AMG) methods have advantages since there memory requirements only increase moderately with increasing DOFs. At the expense of computing time, a pre-conditioner is required. However, Helmholtz equations systems covering large volumes at a high-frequencies may be difficult to solve with conventional GMG and AMG solvers. When solving these types of problems, an effective method is the Complex Shifted Laplacian (CSL) technique. Using CSL, the problem is solved first using a complex wavenumber to pre-condition the Helmholtz equation without damping, while modifying the equation for the preconditioner to improve convergence [17]. Using a state-of-the art computing cluster and the capabilities of MUMPS for frequencies up to 2 kHz and the GMG-CSL approach for frequencies above 2 kHz, the entire frequency spectrum of the SIL4 range of the AW09 helicopter's cabin can thus be covered.

2.4 Acoustic indices

A widespread metric to evaluate interior noise levels in aircraft configurations is the Speech Interference Level (SIL) [19]. It denotes the arithmetic mean of sound levels over specific octave bands covering the frequency range that directly interferes with human speech. Usually, there are two types of SIL levels: At first, the SIL3 value which is the arithmetic mean of the linear sound pressure levels in the 1 kHz, 2 kHz and 4 kHz octave bands and, secondly, the SIL4 level being averaged over the 500 Hz, 1000 Hz, 2000 Hz and the 4000 Hz bands. In the present study, we use the SIL4 which is most commonly used in helicopter applications. An overview of the octave bands contributing to the SIL4 levels is shown in Table 1. The lower frequency limit of each of the octave bands is represented by f_{min} and the upper by f_{max}, respectively. The center frequency of the band is f_c.

TABLE 1: Octave band center frequencies for calculation of the Speech Interference Level (SIL4)

Octave band #	f_{min} [Hz]	f_c [Hz]	f_{max} [Hz]
4	354	500	707
5	708	1000	1414
6	1415	2000	2828
7	2829	4000	5657

3 INSTRUMENTATION

In-flight cabin noise measurements are used in combination with acceleration and vibration probe measurements of the fully instrumented AW09 prototype helicopter. Peak sound pressure levels are obtained from a spectral analysis of the cabin microphone signals. Both data sets are recorded phase-synchronously by the onboard flight-test instrumentation (FTI) system of the aircraft. In the present configuration, a number of 4 cabin microphones (2 in the aft, 1 in the middle and 1 in the front) is used.

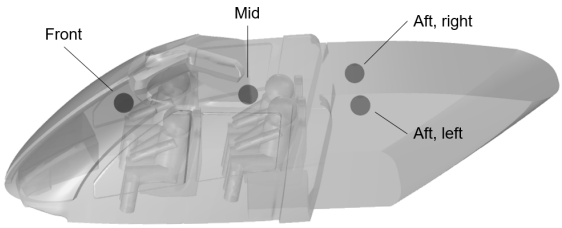

FIGURE 1: Placement of the four microphones inside the AW09 cabin.

The microphones are class 1 omnidirectional microphones of type *Microtech Gefell M 370* with a frequency range between 20 Hz and 20 kHz. The microphones are detachably mounted on fixedly installed cradles to ensure for repeatable measurements at known identical positions. An illustration is given in Figure 1. The microphones in the aft are on flexible mounts attached to the ceiling. The mid microphone is mounted on a support beam of the flight-test instrumentation rack. A minimum distance of 200 mm from any structural element is maintained to avoid unwanted effects from surface reflections. For safety reasons, the front microphone is installed on the overhead panel near the front screen. The minimum distance to structural elements is 150 mm. Noise data is recorded continuously at sampling rate of 32 kHz.

4 MODELING CONCEPT AND METHODOLOGY

The proposed method for simulation of the three-dimensional sound field in the cabin is based on a FEM model of the helicopter cabin. Major noise sources are described by equivalent accelerations computed with a dedicated algorithm based on measurement data. The simulation process can be subdivided into four major steps:

1. Identify peaks from noise spectrum exceeding a certain threshold sound pressure level $L_{\text{p,threshold}}$.
2. For each of the peaks, identify the most likely source of sound.
3. Run a calibration simulation for each source to determine its equivalent acceleration.
4. Transfer source information to design study simulations.

For each of the flight conditions of the rotorcraft of interest, steps 1. – 4. need to be repeated. The required workflow will be described in the following.

4.1 Noise source determination from measurements

In the first step, data from cabin noise measurements are processed. For this purpose, a Fast Fourier

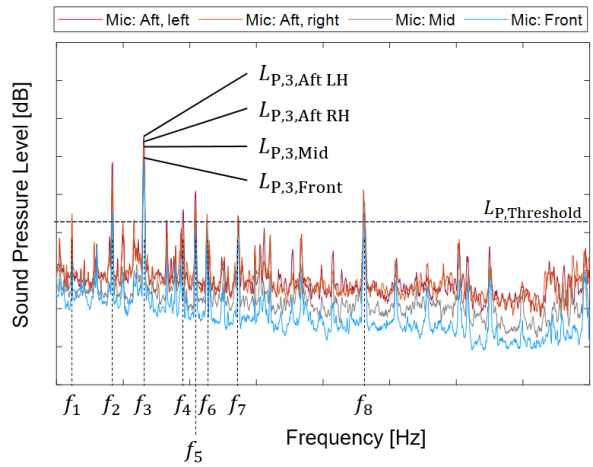

FIGURE 2: Illustration of identification method to select relevant frequency peaks f_i from measured noise spectrum my means of sound pressure level $L_{P,i}$ exceeding the defined threshold value.

Transform (FFT) is applied to the measured time series of the sound pressures at four cabin locations. As an illustrative example, a spectrum for the *Hover* condition is shown in Figure 2. With the objective of focusing on the most relevant sources contributing to the SIL4 level, a certain threshold sound pressure level $L_{P,\text{threshold}}$ is defined to extract the most dominant tones. This means that any peak sound pressure level that is greater than this particular threshold located in the frequency range between 354 and 5657 Hz (see Table 1 for reference) will be selected. Practically this happens by extracting the characteristic frequency and the four peak sound pressure levels at the measurement positions in the manner displayed in Table 2.

TABLE 2: Schema of the table listing all relevant sources with their frequencies and sound pressure level at each measurement position

f [Hz]	$L_{P,\text{Front}}$ [dB]	$L_{P,\text{Mid}}$ [dB]	$L_{P,\text{Aft,L}}$ [dB]	$L_{P,\text{Aft,R}}$ [dB]
f_1	$L_{P,1,1}$	$L_{P,1,2}$	$L_{P,1,3}$	$L_{P,1,4}$
f_2	$L_{P,2,1}$	$L_{P,2,2}$	$L_{P,2,3}$	$L_{P,2,4}$
⋮	⋮	⋮	⋮	⋮

Afterwards, the cross-correlation function $k_{\text{M}_i,\text{A}_j}$ is calculated between each recorded time series of a

microphone i (1 – 4) and each of the acceleration probes j distributed over the instrumented helicopter. As a result, a matrix with the dimensions $N_M \times N_A$ is produced for each frequency allocated to the peaks extracted from Figure 2. In this context N_M corresponds to the number of 4 microphones and N_A to the number of 36 accelerometers. In the next step, the maximum value of the cross-correlation function is determined for each frequency and microphone. For illustration purposes, the results can be displayed as a heatmap, as shown in Figure 3. Based on this, for each frequency column, the sensor at which the correlation function reaches a maximum value is determined. This procedure is repeated for each cabin microphone location. The resulting maximum value is then assigned to the instrumented component / system, which in this example corresponds to the main gearbox. The fact, that all three directions of movements of the accelerometer are among the affected maximum values, the main gearbox is taken as the most likely source of sound for the respective frequency. In case of rotational origin of the source a second verification step is used. For this purpose, the particular frequency is matched with a database of rotational frequencies of the all of the aircraft subsystems. In this case, the rotational speeds of the different transmission stages of the gearbox and their harmonics are used as a plausibility check. The foregoing steps are fully automated by a data processing algorithm implemented in MATLAB®. As a result, tabulated values of frequency, peak sound pressure level at each of the noise measurement locations along with the most likely source component are generated. In practical terms, the data table 2 is complemented with an additional column for the source.

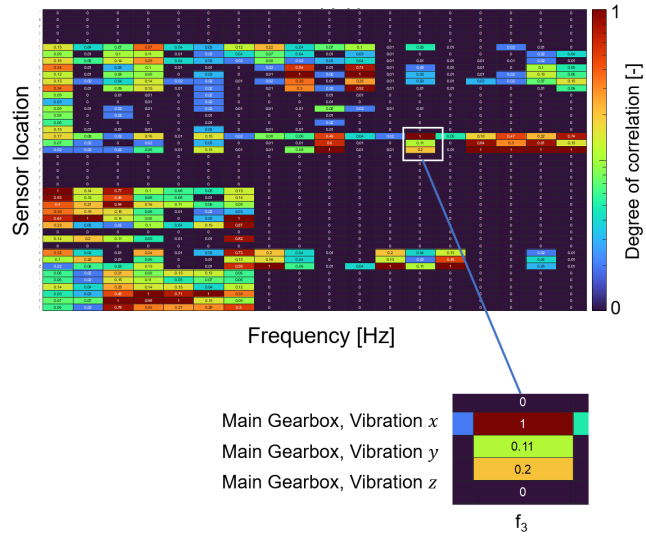

FIGURE 3: Heatmap showing the degree of correlation between vibration probe signals and microphone signal at frequencies exceeding $L_{P,\text{Threshold}}$, representative for one of used cabin microphones.

4.2 Finite Element Model

The simulation approach presented in this study is split into two major parts: Firstly, the sound source identification part and, secondly, the design modelling part. The main purpose of the sound source identification part is to find equivalent acceleration values for each noise source. This happens by exploiting the computed modal distribution of the sound field inside the cabin. In this study, the most relevant sources are defined to be above a certain threshold value of $L_{P,\text{Threshold}}$=75 dB in the frequency range between 354 Hz and 5657 Hz (SIL4-range). For this purpose, the results of the previous analysis steps will be used.

Numerical Set-up The three-dimensional computational domain of the AW09 helicopter's cabin is shown in Figure 4. It represents the cabin inner surfaces of the bare helicopter with seats and passengers. In the present study, the cabin is modeled as symmetric with respect to the middle plane, allowing considerable reductions in computational resources. All bounding surfaces are assumed to be mechanically rigid. Computations are conducted under the premise of weak-coupling between acoustics and structure. Nevertheless, the presented modeling framework already offers the capability of accounting for coupling between structure and acoustics. However, this is planned for the next evolutionary stage of the model. Acoustic sources are employed by impos-

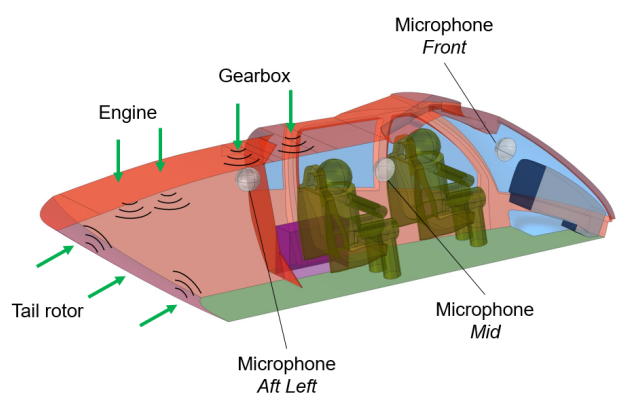

FIGURE 4: Computational domain of the cabin with sources.

ing acceleration boundary conditions at the bounding surfaces. In this specific case, acceleration boundary conditions are used to reflect the main sound sources of the cabin noise signature in the speech-interfering frequency range. For all inner and outer solid surfaces at which no forcing occurs, complex valued and frequency dependent impedances can be implied to represent the acoustic reflection and absorption properties of the respective material. In addition and especially relevant for analyzing interior trim panels and linings acoustic transmission properties can be modeled by accounting for transfer impedance and surface impedance using transfer matrices.

Discretization and mesh The volume of the cabin is discretized with a tetraeder mesh having at least six elements per wavelength. The level of detail of the model is tailored in such a way that objects with $V << V_{\text{cabin}}$ are neglected, whereas objects with larger volumes such as seating, crew/passengers and large equipment reflect the real configuration as close as possible. To optimize the performance of the meshing, this is realized by a subdivision of the grid size into discrete ranges. For example, for all frequencies considered below 1500 Hz, a resolution of 6 elements per wavelength corresponding to:

$$l_{max} \leq \frac{c}{1500\,\text{Hz}} \tag{9}$$

is used. For all frequencies $1500 < f \leq 2500$ Hz, the maximum allowed element size corresponds to 6 elements per wavelength at a frequency of 2500 Hz and so on. The number of elements of the computational grids used in this study range between $\approx 750\,000$ for frequencies within the 4th octave band and up to ≈ 7 million elements for the 7th octave band.
An illustrative example of the mesh is displayed in 5. The acoustic field is then calculated using the discretized formulation of the Helmholtz equations in frequency space (Eq. 3). The medium inside the cabin is defined as dry air at a temperature of $T = 293.15\,\text{K}$. For frequencies up to 2.5 kHz, a Multifrontal Massively Parallel Sparse Direct Solver (MUMPS) solver is used. For frequencies above 2.5 kHz, the model is solved with an iterative approach that uses the Complex Shifted Laplacian method (CSL).

4.3 Computation of equivalent noise sources

As input parameters for the following step, the data table containing peak frequencies, source location and peak sound pressure level for each microphone is used. The basic idea behind this is to determine an equivalent acceleration for each source which, taking into account the sound field inside the cabin,

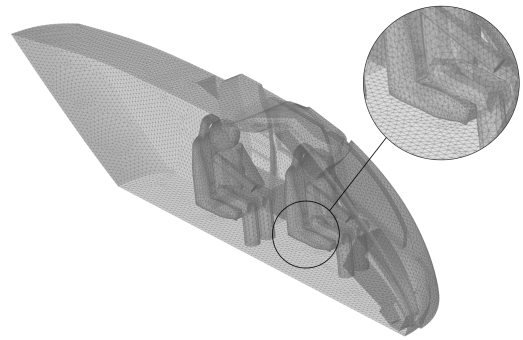

FIGURE 5: Section view showing the computational grid for the AW09 helicopter cabin.

matches the measured sound pressure levels for each of the reference locations. For this purpose, each frequency listed in table (compare Figure 2) is treated separately. These acceleration values $a_j(f)$ will be termed *equivalent accelerations*, in the following. Similar methods are e.g. described in [15] and [16]. The process flow used for the present study is schematically shown in Figure 6.

The determination of the equivalent accelerations is carried out with the FEM model described in Section 4.2. To this end, the arrangement of the seats and crew is aligned as closely as possible with that of the test flight carried out. For each frequency, forcing is realized by employing a constant acceleration $a(f)$ value to the location of the respective component. Using the main-gearbox (MGB) as an illustrative example, the surface area at which the equivalent acceleration is employed corresponds to the area at the upper deck located below the projected surface of the MGB outer contours. In this case, the normal acceleration is applied to the cabin geometry's outer surface. An illustration of the acceleration force with respect to the cabin model is shown in Figure 7. In this presented version of the model, all structural elements are assumed to be rigid and weak coupling to the fluid is presumed. Therefore, the forcing only acts as an acoustic source without coupling to the structural mechanics. However, note that the set-up in a multiphysics simulation environment has great extension potential. For example, structural-acoustic interfaces can be simulated while taking material properties into account. In case transfer path analyses from the sources to the cabin are available, these may also be integrated. Since the presented approach intends initially to exploit data generated during regular prototype flight test operations with minimal additional measurement effort, the obtained information on the sources has certain limits.
To reduce the sensitivity against local deviations es-

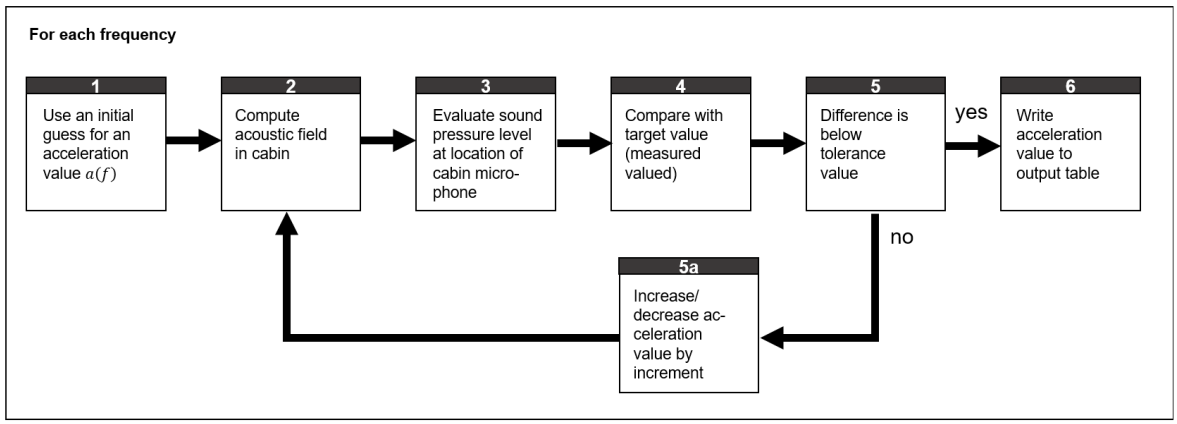

FIGURE 6: Flow chart for the determination of a equivalent acceleration values for the noise sources.

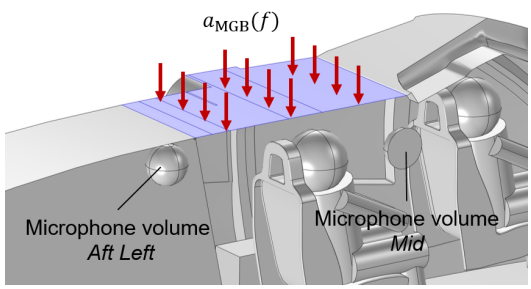

FIGURE 7: Equivalent acceleration of the main gearbox (MGB) applied to the outer surface of the helicopter cabin.

pecially at high frequencies, the locations at which the sound pressure levels are referenced is a volumetric average of a sphere with a radius of $r_{\mathrm{M}} = 0.1\,\mathrm{m}$ with the origin being the exact microphone location. The cabin arrangement used as geometric reference for the simulation is the bare AW09 helicopter. In order to describe the bare helicopter, sound-hard walls are assumed in each case, which is achieved by setting the wall impedance equal to:

$$Z_{\mathrm{wall}} = \infty. \tag{10}$$

The acoustic properties of surfaces of seats and crew are resembled by surface impedances for leather and textiles from literature. The process flow of the source estimation algorithm is outlined as a process flow shown in Figure 6. Using one of the frequencies, identified as a gear-meshing frequencies of the main-gearbox (MGB) exceeding a certain threshold level. For the algorithm an initial guess of $a_{\mathrm{MGB}}(f_i) = 0.1\,\mathrm{m/s^2}$ has been found to be practicable (step 1). Having now all boundary conditions defined, the three-dimensional acoustic field inside the cabin is computed for the frequency f_i using the Helmholtz equations (Eq. 3), (step 2). Afterwards, the resulting sound pressure levels are evaluated by means of a volumetric average of the spheres coinciding with each of the four microphone measurement locations (step 3). In step 4, the difference between the computed sound pressure levels at the microphone locations and the measured values (see Table 2) is calculated. A Newton-Raphson-like method is used to iterate an acceleration value $a_{\mathrm{MGB}}(f_i)$ to satisfy a maximum deviation between the simulated and measured value at the microphone positions (step 5):

$$\left| L_{\mathrm{P,measured,M}_i}(f_i) - L_{P,\mathrm{sim,M}_i}(f_i) \right| \leq 0.1\,\mathrm{dB}. \tag{11}$$

Where $L_{P,\mathrm{meas,M}_i}(f_i)$ represents the measured sound pressure level at one of the available cabin microphone locations and $L_{P,\mathrm{sim,M}_i}(f_i)$ is the corresponding numerically simulated value. The algorithm is converged, when the condition given by Equation 11 is satisfied. The iteration routine completes with writing the determined acceleration value $a_{\mathrm{MGB}}(f_i)$ to an output table (step 6). This procedure is carried out for all other entries of Table 2 containing the targeted values of $L_{P,i}$ for each microphone at the characteristic frequencies of the sources considered most relevant. In the presented study, the forcing locations are selected analogously per component group. Using the above described procedure, one obtains tabulated equivalent acceleration values are considered representative to the particular flight condition of the helicopter for the cabin in flight test configuration. These acceleration values depending on location and frequency are further used as boundary conditions for subsequent design studies.

5 RESULTS

In the following, simulation results of design studies are discussed. All results are representative for the AW09 prototype helicopter in the flight condition *Hover*. For this purpose, substitute noise sources have been determined by means of equivalent accelerations from microphone measurements in Hover as outlined in Section 4. Within the SIL4 range, a number of 13 frequencies are considered at which the sound pressure levels exceed the chosen limit of 75 dB. In total 7 of these frequencies have been attributed to the main gearbox, 3 to the engine and another 3 to the tail-rotor. Note, that only tonal noise sources that can be clearly assigned to their origin by their characteristic frequency and correlation to a vibration signal were considered here. For each of the octave bands contained in the SIL4-range, i.e. 500 Hz, 1000 Hz, 2000 Hz and 4000 Hz one representative frequency is chosen to illustrate the acoustic pressure distribution in the cabin. For example, $f_{\text{oct4,1}}$ corresponds to the first relevant source within the 4th octave band with a center frequency of f_c=500 Hz. Finally, to assess the effectivity of acoustic measures in the cabin, results are displayed in terms of offset from the sound pressure level to the bare helicopter configuration for each of the four relevant octave bands. A negative number means a decrease of the noise levels with respect to the baseline configuration.

Three cabin configurations were considered: At first, the existing, bare flight test configuration used to calibrate the levels and, secondly, a possible cabin configuration with integrated carpet and, thirdly, with carpet and a ceiling panel. In all cases, four passengers are located in the aircraft. Pilot and co-pilot in the front row and two additional crew members in the rear. In the presented study, a half-model of the cabin is used and symmetry is exploited with respective center plane between the nose and the aft of the aircraft.

Acoustic boundary conditions for the windows, seats and passenger surfaces are assigned using real-valued sound absorption coefficients. The values for α are obtained from a cubic interpolation scheme as a function of the frequency (see Figure 8, data taken from [21]). For the source calibration model, all other surfaces are modeled as sound-hard ($\alpha = 0$). For design studies, the acoustic properties of carpet and ceiling panel are as well represented by cubical interpolation functions based on tabulated absorption values (see Figure 8). Note that these absorption coefficients only describe the real part of the specific acoustic impedance Z_i for the corresponding surfaces. Since we consider only frequencies within the SIL4 range for which the lowest covered frequency is 354 Hz (lower frequency bound of the 500 Hz octave band), this simplification is considered acceptable.

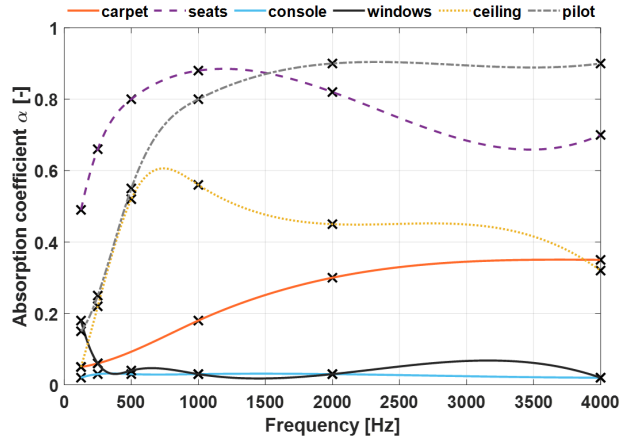

FIGURE 8: Acoustic absorption coefficients of materials used in the cabin from literature [21] with cubic interpolation functions.

For the given numerical set-up, the simulation time varies between approx. 1 minute per source in the 4th octave band and up to approx. 15 min per source for frequencies within the 7th octave band. In total, we found that around 30 – 45 min are required for one configuration of the AW09 helicopter including meshing and pre-conditioning of the system matrices when employing 13 noise sources within the SIL4 range.

Figure 9 shows a set of contour plots representing the normalized acoustic pressure on a cut plane from the front to the aft of the cabin. Contours are shown for each one representative acoustic field pressure field. Using different sets of boundary conditions, either the bare helicopter or the helicopter equipped with carpet and a generic, absorbing ceiling panel is represented. The excitation source which corresponds to the results shown for $f_{\text{oct,4}}$ is the engine. The results shown for the the frequency bands $f_{\text{oct,5}}$-$f_{\text{oct,7}}$ are based on the excitation by different gearbox meshing frequencies. Considering the results for $f_{\text{oct,4}}$ corresponding to the bare helicopter, a rather diffuse spatial distribution of the acoustic pressures can be observed. Higher overall sound pressure levels in the aft can be explained by the vicinity of the excitation locations acting on the outer roof surface. From the depicted pressure distribution with carpet and ceiling, a shift of the pressure maxima and minima in the aft is clearly visible, while amplitudes in next to the pilots and the cockpit

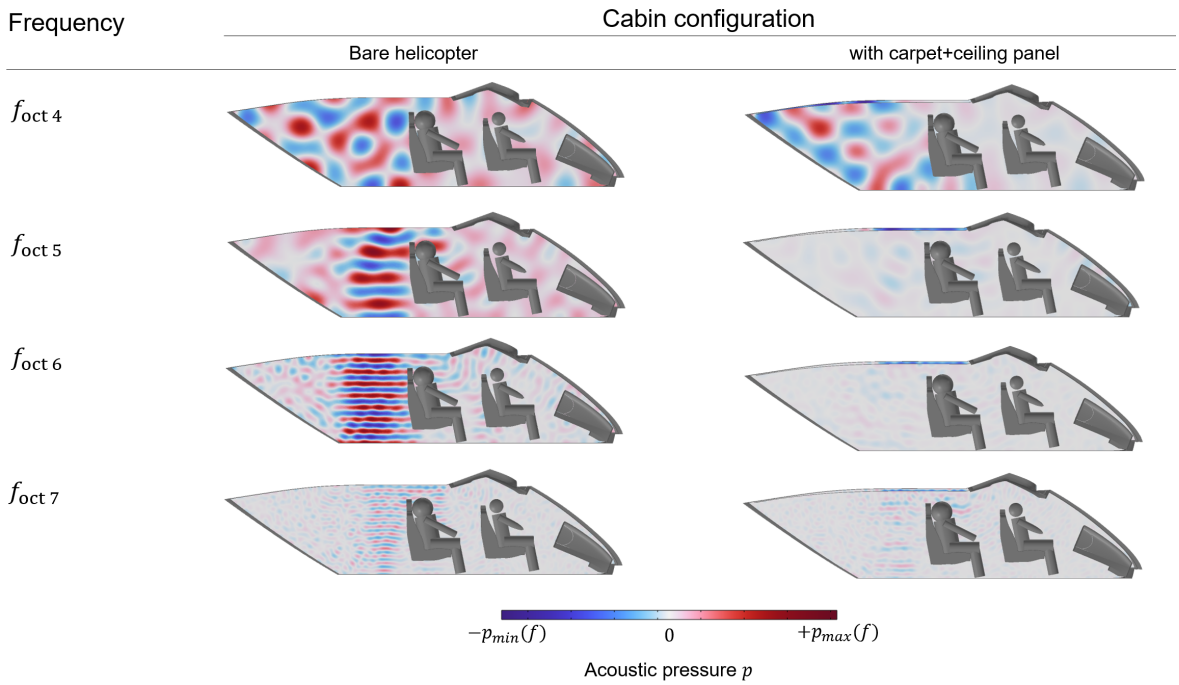

FIGURE 9: Normalized acoustic pressures for one representative frequency per octave band on a cut-plane through the helicopter cabin.

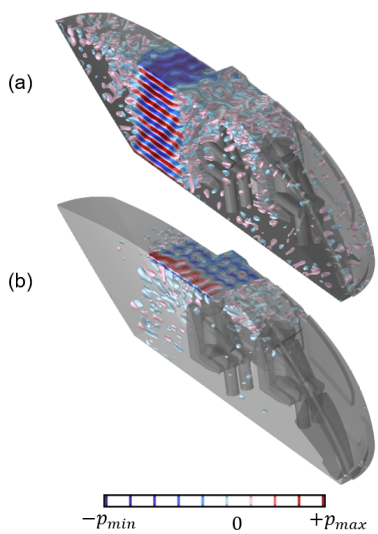

FIGURE 10: Isosurfaces of acoustic pressure inside the cabin being excited at a frequency allocated to the gearbox within the 7th octave band.

decrease noticeably. This observation suggests that the combination of the noise source and the roof panel thus influences the acoustic mode in such a way that the noise mitigation has a more pronounced effect on the front area. A different picture is seen for the mode shapes computed for the frequencies $f_{\mathrm{oct},5}$-$f_{\mathrm{oct},7}$. For the bare helicopter, the acoustic pressure distributions reveal a transversal pattern between the ceiling and the floor. This suggests a transversal mode in the cubic volume right behind the passenger seats. This is particularly noticeable for the pressure contours representative for the 5th and the 6th octave band, respectively. In turn, a transversal mode is still indicated in the case of the 7th octave band. However, the mode shape indicates a higher attenuation than for the previous frequencies, which can be attributed to the higher dissipation associated with the higher frequency. Considering the mode shapes with carpet and ceiling panel displayed in the right-hand column of Figure 9, clear distinctions can be seen compared to the bare helicopter case. In particular, for the displayed mode shapes within the 5th and 6th octave band the pressure distribution appears more distorted while the highest pressure amplitudes are observed in the gap between the ceiling and the panel upper surface. This effect is further illustrated in Figure 10. The figure shows isosurfaces of the acoustic pressures in a three-dimensional section view of the cabin. From this, it can be seen for the gearbox excitation at a frequency within the 6th octave band, that a spatial propagation of the acoustic mode is effectively suppressed by the ceiling panel. For the gearbox excitation in the 7th octave band also a

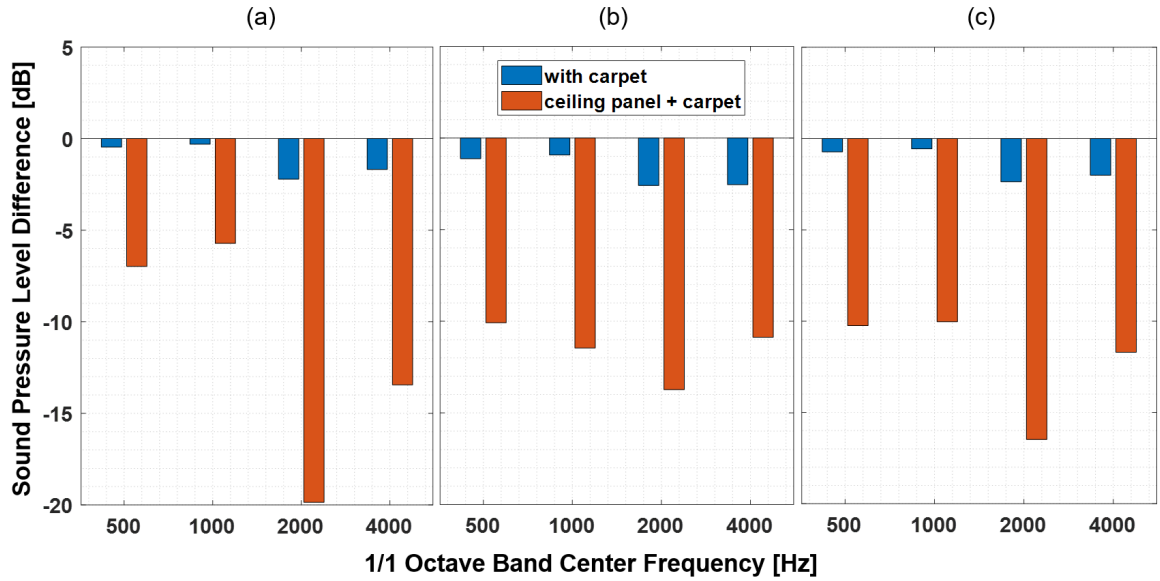

FIGURE 11: Predicted reduction of sound pressure level for octave bands 4 – 7 averaged for the aft (a) and front (b) compartment and for the (c) overall helicopter cabin with carpet and ceiling panel+carpet.

reduction of the acoustic pressure amplitudes along with a more pronounced distortion of the mode shape is predicted.

In the next step, the global effectivity of the two proposed measures will be assessed. For this purpose, two metrics will be considered: At first, the sound pressure levels for each four of the octave bands relevant for the SIL4 acoustic metric and, secondly, the SIL4 levels itself. The levels in the aft and in the front are particularly relevant for passenger comfort. Therefore, the respective metrics are discussed for a volumetric average across the aft of the cabin where passengers are seated, for the front area, where pilots are located and also over the entire cabin volume. Using the bare helicopter as the reference configuration, all sound pressure levels are presented relative to this reference case. This is realized by means of the sound pressure level difference in dB, while a negative offset means a reduction with respect to the bare helicopter case and vice versa.

The results for the sound pressure level reductions per octave band are shown in Figure 11. The figure shows the sound pressure levels for the octave bands 4 – 7 for the aft (a), the front (b) and the overall cabin volume (c). As shown in the figures, the impact of the carpet on the sound pressure levels is severely lower than for the ceiling panel. This is indeed an expected result since the carpet only reduces the noise reflection on the floor which is located far from the most relevant sources. The computed noise reduction attributed to the carpet lies between approx. 0.3 and 0.5 dB in the aft for the 500 and 1000 Hz octave band and between approx. 1.7 and 2.2 dB for the 2000 and the 4000 Hz band in the aft compartment. The greater reduction for higher frequencies can be explained by the increase of the carpet's absorption coefficient with increasing frequency. In addition, the carpet's effect on the sound pressure levels is more pronounced for the front compartment than for the aft compartment. In particular, for the front compartment the numerically calculated noise reduction lies between approx. 0.9 and 1.1 dB for the 500 and 1000 Hz octave band and between at approx. 2.5 dB for both the 2000 Hz and the 4000 Hz band, respectively. On average, the highest noise level reduction of the carpet over the entire cabin volume is predicted for the 2000 Hz band with approx. 2.4 dB. The reduction potential of the generic ceiling panel reveals a frequency dependency as well as a local dependency. Reductions of the sound pressure levels computed with the presented model range between approx. 5.7 dB for the 1000 Hz band in the aft compartment up to approx. 20 dB for the 2000 Hz band as well in the aft compartment. The reduction potential for the 4th and the 5th frequency band is found to be lower in the aft compartment ($\approx$ 5.7 – 7 dB) than in the front area ($\approx$10 – 11.5 dB).

Figure 12 shows the computed reduction potential for the Speech Interference Level (SIL4). The displayed

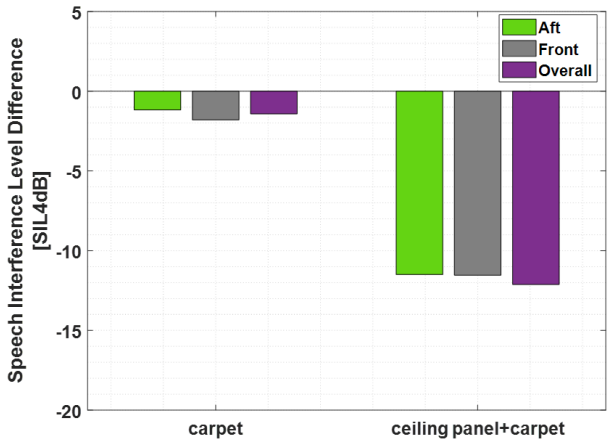

FIGURE 12: Computed influence of the measures carpet and ceiling panel + carpet on the SIL4 levels averaged over the aft and front compartment and for the entire helicopter cabin.

results are grouped by the type of measure (carpet or carpet+ceiling panel) and by location in the cabin (aft, front or overall cabin averaged). For the used configuration, the predicted reduction of the SIL4 level for the carpet lies between $\approx$ 1.2 and 1.8 dB compared to the bare helicopter configuration. In general, the effectivity of the carpet seems to be greater in the front compartment of the helicopter. Regarding the combination of the carpet and a generic ceiling panel, the decrease of the SIL4 levels is computed to approx. 11.5 dB. The reduction is found to be similar for the aft and the front compartment.

6 CONCLUSIONS AND OUTLOOK

In the presented paper, a comprehensive methodology to predict the noise level reduction potential of two selected, passive measures in a helicopter cabin has been presented. By using the AW09 helicopter as a practical application, it has been demonstrated how interior noise measurements obtained with little additional effort during regular flight test operations were used to derive the source strength of the most relevant noise sources. A practical approach to determine the most likely origin of the noise sources has been presented. Based on a sound pressure level threshold of 75 dB, 13 noise sources within the SIL4 range were identified. For each of these sources, equivalent accelerations were computed and imposed as forcing boundary conditions in a three-dimensional FEM-based simulation model of a helicopter cabin. Within the scope of this is study it emerged that all frequencies within the SIL4 range can be covered by the presented comprehensive simulation model. The computational time per configuration covering all 13 sources was in the order of magnitude of 30-45 min. Decisive enablers for this were modern direct and iterative numerical solvers for the Helmholtz equations while a pre-conditioner was used to extend the frequency range to larger frequencies. The practical applicability to real interior design was demonstrated by studying the sound field for the case with carpet as well as the combination of carpet and ceiling panel. The materials were acoustically described by frequency-dependent absorption coefficients from literature.

In contrast to the use of conventional methods like SEA, the presented approach allowed to directly quantify the influence of acoustic measures on the sound pressure levels at any location in the cabin. With this model, the SIL4 reduction potential of the chosen carpet has been predicted between $\approx$ 1.2 and 1.8 dB while up to approx. 11.5 dB was found for the ideal ceiling panel.

Due to its implementation in a multiphysics simulation platform, the presented interior noise model offers a high degree of flexibility and potential for further extensions. As a first step, further development of the yet coarse description of the sources is planned. For this purpose, methods such as transfer path analysis as well as methods of inverse FEM using microphone array measurements are under consideration. With this information, the local dependency of the sources shall be resolved finer and specified more accurate. In this way, it would also be feasible to implement leakages and other unforeseen sources. Furthermore, the options to include a broader scope of acoustic treatments will be continuously extended. If available, surface absorption and transmission losses of materials can be described and implemented based on their acoustic transfer matrix. These can be implemented using either manufacturer data, impedance tube measurements, or separate numerical simulations. With the presented high-fidelity simulation model, there is also the potential to consider new types of materials such as acoustic metamaterials.

ceedings and for inclusion in a freely accessible web-based repository.

REFERENCES

[1] Wilby, J., and Smullin, J., 1979. "Interior noise of STOL aircraft and helicopters". *Noise Control Engineering Journal,* ***12***(3).

[2] George, A. R., 1978. "Helicopter noise: State-of-the-art". *Journal of Aircraft,* ***15***(11), pp. 707–715.

[3] Jedliński, Ł., 2016. "A new design of gearboxes with reduced vibration and noise levels". *Diagnostyka,* ***17***.

[4] Scheidler, J. J., 2016. "A review of noise and vibration control technologies for rotorcraft transmissions". In INTER-NOISE Congress Proceedings, Vol. 253, Institute of Noise Control Engineering, pp. 2986–2997.

[5] Tuma, J., 2009. "Gearbox noise and vibration prediction and control". *International Journal of Acoustics and Vibration,* ***14***(2), pp. 1–11.

[6] Marburg, S., 2002. "Six boundary elements per wavelength: Is that enough?". *Journal of Computational Acoustics,* ***10***(01), pp. 25–51.

[7] Davis, E. B., 2005. "By air by SEA". *Journal of Sound and Vibration,* ***39***(7), pp. 12–17.

[8] Campolina, B., 2012. "Vibroacoustic modelling of aircraft double-walls with structural links using statistical energy analysis (SEA)". PhD thesis, Université de Sherbrooke; Université Pierre et Marie Curie-Paris VI.

[9] Peiffer, A., and Tewes, S., 2008. "Interior noise prediction of aircraft section using hybrid fem/sea methods". In INTER-NOISE Congress and Conference Proceedings, Vol. 2008, Institute of Noise Control Engineering, pp. 938–948.

[10] Cotoni, V., Shorter, P., and Langley, R., 2007. "Numerical and experimental validation of a hybrid finite element-statistical energy analysis method". *The Journal of the Acoustical Society of America,* ***122***(1), pp. 259–270.

[11] Mucchi, E., and Vecchio, A., 2009. "Experimental transfer path analysis on helicopters". In Proceedings of the International Conference on Acoustics (NAG/DAGA2009), Rotterdam, Netherlands, pp. 23–26.

[12] Mucchi, E., and Vecchio, A., 2013. "Experimental vibro-acoustic transfer path analysis on helicopters". In International Design Engineering Technical Conferences and Computers and Information in Engineering Conference, Vol. 55997, American Society of Mechanical Engineers, p. V008T13A008.

[13] Lahaye, D., Tang, J., and Vuik, K., 2017. *Modern solvers for Helmholtz problems*. Springer.

[14] Kun, J. C., and Feszty, D., 2019. "Review of finite element vehicle interior acoustic simulations including porous materials". *Acta Technica Jaurinensis,* ***12***(3), pp. 218–236.

[15] Anderssohn, R., Großmann, C., et al., 2006. "FEM-based reconstruction of sound pressure field damped by partially absorbing boundary conditions". *Mechanics Research Communications,* ***33***(6), pp. 851–859.

[16] Weber, M., Kletschkowski, T., and Sachau, D., 2008. "Identification of noise sources by means of inverse finite element method using measured data". *Journal of the Acoustical Society of America,* ***123***(5), p. 3064.

[17] COMSOL Multiphysics®, Version 6.0, 2021. Reference manual.

[18] Pierce, A. D., and Beyer, R. T., 1990. *Acoustics: An introduction to its physical principles and applications*. Acoustical Society of America.

[19] Dreher, J. J., and Evans, W. E., 1960. "Speech interference level and aircraft acoustical environment". *Human factors,* ***2***(1), pp. 18–27.

[20] Operto, S., 2021. "Up-to-date assessment of 3D frequency-domain full waveform inversion based on the sparse multifrontal solver mumps". In Fifth EAGE Workshop on High Performance Computing for Upstream, Vol. 2021, European Association of Geoscientists & Engineers, pp. 1–5.

[21] DIN18041-2016-03, 2016. Hörsamkeit in Räumen - Anforderungen, Empfehlungen und Hinweise für die Planung.